

Role of Lithology and Subsurface structures detected by potential field data in controlling the radioactive mineral accumulation at Natash area, Eastern Desert, Egypt

Shadia Elkhodary* and Taha Rabeh

Received: September 03, 2013; accepted: October 15, 2013; published on line: July 01, 2014

Resumen

La zona de Wadi Natash se encuentra en la parte sur del desierto del este de Egipto. Tiene una gran importancia, ya que cuenta con gran acumulación de minerales radiactivos, como uranio, torio y potasio. En esta zona se llevó a cabo un estudio de potencial integrado, con el objetivo de localizar a profundidades factibles cuerpos con susceptibilidad magnética suficiente para representar intrusiones magmáticas relacionadas con la radioactividad del lugar y delinear las estructuras del subsuelo que afectan la zona. Tanto los datos magnéticos y de Bouguer como los datos radiométricos se interpretaron rápidamente por la posición de la fuente y las profundidades. Lo anterior fue factible al utilizar la deconvolución de Euler y de Werner, además de técnicas de modelado en 3D. Los resultados deducidos del análisis de tendencias muestran que la tendencia de la falla principal que afecta a la zona tiene una dirección de NNW-SSE (Mar Rojo-Golfo hacia Suez) y atraviesa por el menos predominante NNE-SSW (El Golfo de Aqaba-dirección Mar Muerto) y por WNW-ese (sistema de falla Najd). Los organismos causantes fueron fotografiados a profundidades que van de 0,3 kilómetros hasta 1,5 km. Las profundidades a lo largo de las discontinuidades se deben a la presencia de la falla NNW-SSE y actúan como canales de paso para las soluciones hidrotermales.

Puede afirmarse que las acumulaciones de minerales radiactivos fueron causadas por las soluciones hidrotermales ricas en minerales radiactivos como resultado de la intrusión volcánica Natash a las rocas graníticas. Los clásticos Qouseir y la piedra de la arena Nudian se vieron afectados por estas soluciones y muestran una respuesta positiva de los minerales radiactivos.

Key words: magnético, litología, minerales radiactivos, modelo magnético en 3D.

S. Elkhodary
Geology Department
Faculty of Science
Tanta University
Tanta, Egypt

*Corresponding author: S_elkhodary@hotmail.com

Abstract

Wadi Natash area is located in the southern part of the Eastern desert of Egypt. It has a great importance for containing accumulations from the radioactive minerals of Uranium, Thorium and Potassium. An integrated potential study was carried out on the study area with the aim of locating depths to causative bodies with sufficient magnetic susceptibility that may represent magmatic intrusions with relation to the radioactivity location and delineate the subsurface structures affecting the area. Both magnetic and Bouguer data as well as radiometric data were interpreted rapidly for source positions and depths using Euler deconvolution, Werner deconvolution and 3D modeling techniques. The results deduced from the trend analyses show that the major fault trend affecting the area have NNW-SSE (Red Sea-Gulf of Suez trend) direction intersected by the less predominant NNE-SSW (The Gulf of Aqaba-Dead Sea trend) and WNW-ESE (Najd Fault System) fault trends. The causative bodies were imaged at depths ranging from 0.3 km to about 1.5 km. The depths along the interpreted profiles display discontinuities in potential field markers due to presence of the NNW-SSE fault trends act as pass channels for the hydrothermal solutions.

It can be stated that the radioactive mineral accumulations were caused by the hydrothermal solutions rich with radioactive minerals as a result of intruding Natash volcanic to the granitic rocks. The Qouseir clastics and the Nudian sand stone were affected by these solutions and show a positive response for the radioactive minerals.

Key words: magnetic, lithology, radioactive minerals, 3D magnetic model.

T. Rabeh
National Research Institute
of Astronomy and Geophysics
Cairo, Egypt

Introduction

The area under study is located in south Eastern Desert. It is delineated by longitudes 33° 00' to 34° 30' E, and latitudes 24° 00' and 25° 00' N (Figure 1). Wadi Natash volcanics cropped out in different spots at the eastern part of the investigated area as alkaline basalts and some small trachytic intrusions which erupted during the Upper Cretaceous associated with regional uplift preceding the northern Red Sea rifting (Figure 1).

This study deals with an integrated interpretation of the observed aeromagnetic and gravity data of Wadi Natash area based on application of gradient (Euler, Werner deconvolution, trend analysis and three dimensional modeling) methods to study the effect of subsurface structures and lithology in controlling the radioactive accumulations.

Geologic Setting

The considered area is topographically graded between gentle to rough topography which traversed by many wadis trending NE-SW, NW-SE, WNW and E-W controlled by the structural directions and the rock types of the area.

The study area is covered with a variety of basement and sedimentary rocks ranging in age from Precambrian to Quaternary (Figure 1). Precambrian rocks consist of acidic metavolcanics (MVa), metasediments (MS) and calc-alkaline granites (ga and gβ) cover the southern eastern part of the area. The northern eastern part of the area is covered by Upper Cretaceous volcanics (wadi natash volcanics) and trachyte plugs (Hashad, *et al.*, 1982). Meanwhile, the Upper Cretaceous Nubian sandstones cover the central and western parts of the area represented by (Abu-Aggag (Ku) and Um Barmil (Kub) Formations). Late cretaceous shall and limestone represented by Dakhla (kud) and Kiseiba (Tpl) occupying the northwestern corner of the area, (Conoco Report, 1989).

One of the extensive lava fields in the East Sahara Swell is that of Wadi Natash in the southern Egypt. Natash volcanics crop out in the study area at the southeastern corner, northeastern, northwestern, and southwestern corners of the study area. The volcanic rocks and their volcaniclastic sediments are nearly parallel to the boundary between the (upper and lower) Nubian sandstones. The lava flows form a dissected plateau with a stratified appearance which trends NNW-SSE. This plateau is formed of thick piles of volcanic flows; each of them extends laterally for more than 6km. They also include a number of cones and sills of olivine basalt. The cones are cone-shaped features, rising up to 26-86 m above wadi level, while sills are always encountered in the Nubian Formation in the form of flat lying bodies interbedded with the sandstones and measure up to 7m in thickness (Hashad, *et al.*, 1982). Ibrahim (2010) records for the first time the occurrence of laterites-bearing REEs in Natash area which form as horizons at the boundary between the Cretaceous sandstones and Natash flows.

The volcanic sequence is represented by three distinct flow unites, separated by two sequences of volcaniclastic sediments. Each of

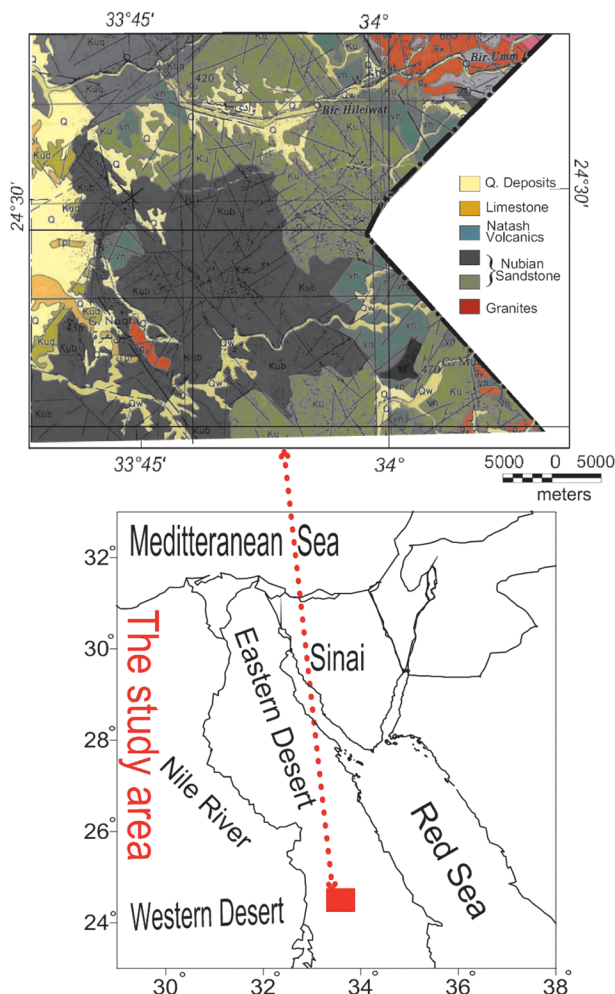


Figure 1. Location map and surface geologic map of the study area after CONOCO (1987).

the tree flow unites shows a gradual change in composition upwards from alkali olivine basalts through trachybasalts, trachyandesite, to trachytes. The volcaniclastic sediments comprise agglomerates and tuffs which contain leaf imprints of Cenomanian age (Crawford *et al.*, 1984), which are in good agreements with a 90Ma K-Ar age for the lavas determined by Ressetar *et al.*, (1981). The age of these volcanics suggests that they are not directly associated with the actual mid-Tertiary Red Sea rifting but their alkaline nature implies that they were involved with a pre-rifting doming process (Crawford, *et. al.*, 1982).

Structurally, Noweir, *et al.* (2003) concluded that the rocks of Wadi Natash have general linear trend outcrops conformable with the general structure trend. The linear trend suggests that these volcanic bodies were brought up along the intersection of the main NNW to NW fault trend with the E-W fault direction during the Turonain age.

Potential field data acquisition

An aeromagnetic survey conducted by Aero Service, (1984) was used to interpret the regional subsurface structures prevailing in the study area along with gravity data obtained from the 1-arc-minute gravity anomaly (mGal) grid by Sandwell and Smith (1997). The aeromagnetic survey was flown at 1km altitude with north-east flight lines every 1 km and tie-lines every 10 km in perpendicular directions to the flight lines. The aircraft was equipped with a tail-stinger of non-magnetic plastics of 1.5 meters long at the rear of the fuselage. The magnetic data were digitized by computer digitizing programs and both Bouguer and the total magnetic anomaly map were obtained (Figures 2 and 3).

Potential field data processing

The aeromagnetic data was digitized into a computer using a suitable Surfer Program v. 8.00 (Surfer, 2002). The first step in data

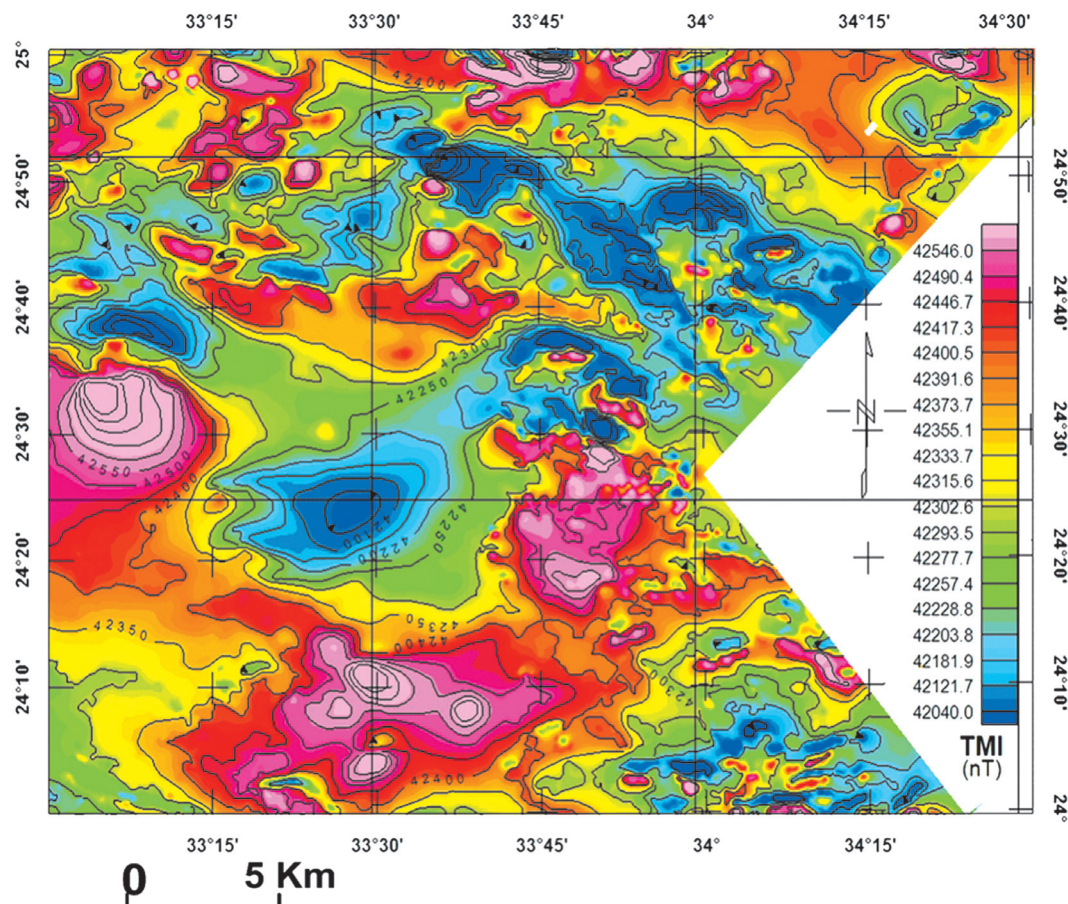


Figure 2. Total Intensity aeromagnetic map of study area (after Aero Service, 1984).

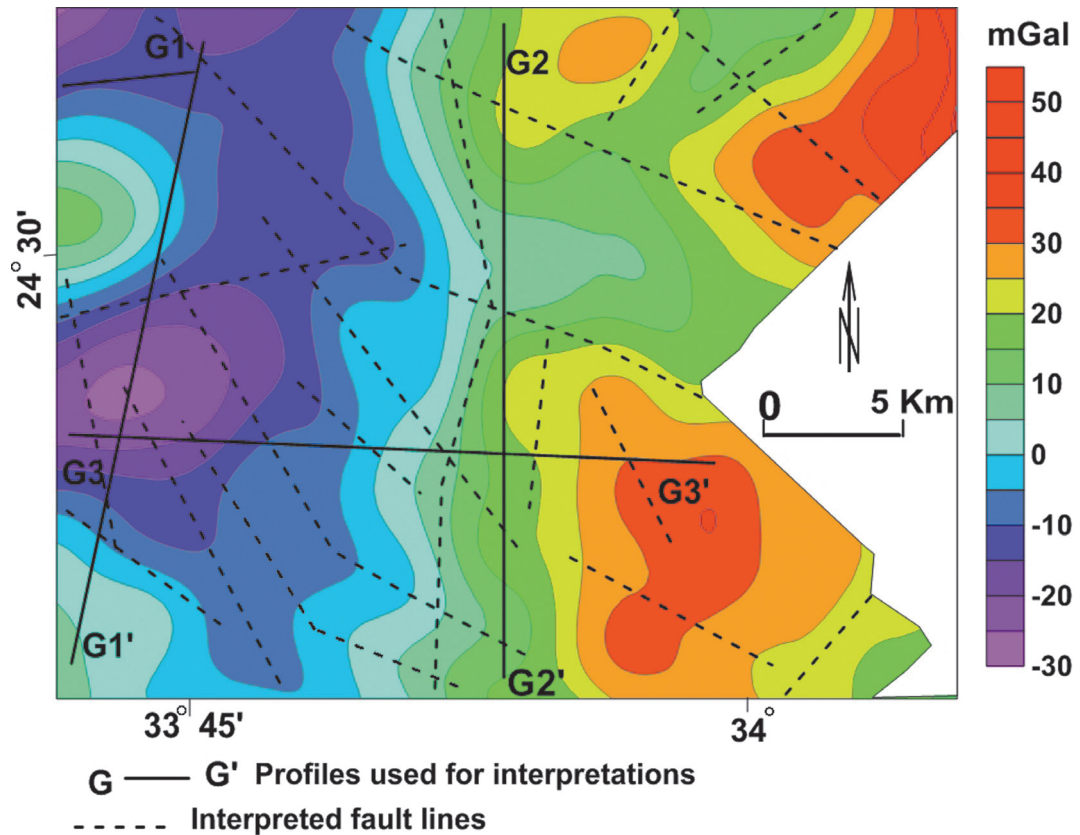


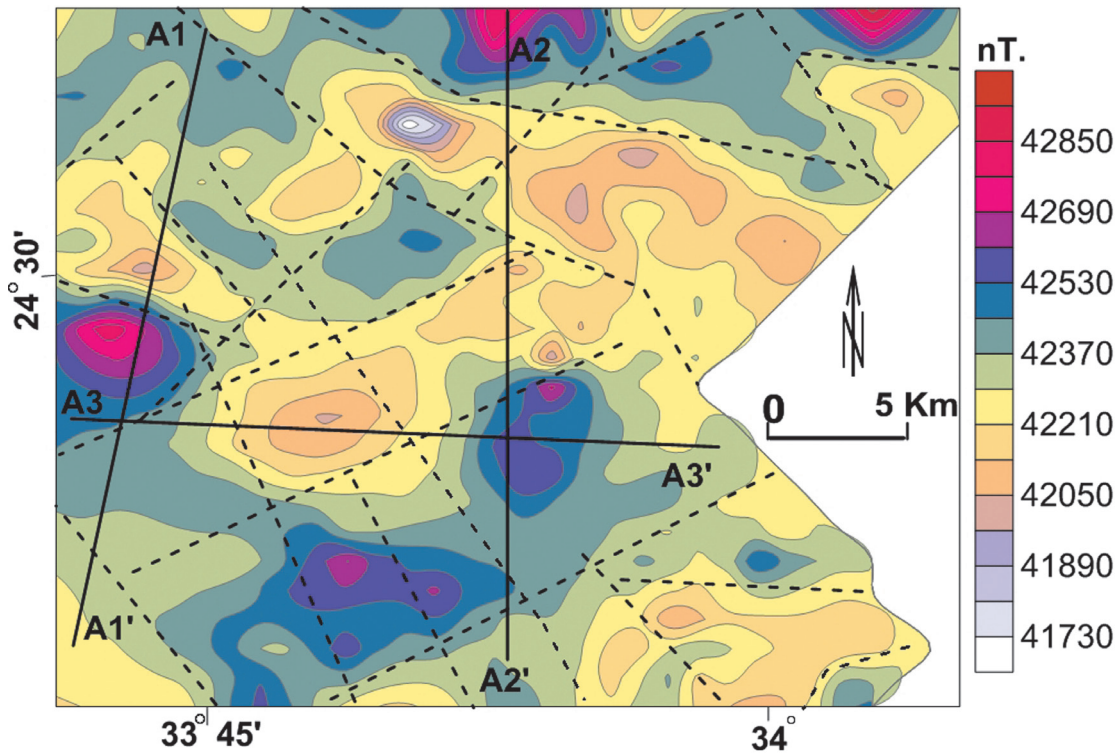
Figure 3. Bouguer anomaly map of the study area (after Sandwell and Smith, 1997) showing profiles and deduced fault trends.

processing was reduction to the magnetic north pole (RTP). This procedure has the advantage of compensating for the shift between sources and magnetic anomalies due to the non-verticity of both the normal field and the magnetization. Only induced magnetization was considered. Inclination and declination of the normal field were fixed at 32.8 N and 1.9 E. RTP was conducted in the Fourier domain (Blakely, 1995). The results are presented in (Figure 4) for the aeromagnetic survey. Both the Bouguer anomaly and the RTP aeromagnetic maps (Figures 3 and 4) indicate that most anomalies are aligned to NW, NE, and E-W which may be related to the Red Sea, and Gulf of Aqaba tectonics. The negative anomalies in the central part may be due to deep depths to the basement rocks or the lithology of negative magnetic effects.

The RTP aeromagnetic anomaly map (Figure 4) shows low and high frequency magnetic anomalies distributed along the study area. The elongated positive magnetic anomalies with a maximum value of 42850 nT were observed over the locations of southwest, west and north the study area. They are characterized

by high frequency and high amplitude. Such magnetic anomalies are associated with acidic metavolcanics, metasediments and calc alkaline granites, Natash volcanic which are mainly characterized by high magnetic susceptibilities. These magnetic anomalies are bounded by steep magnetic gradients, which indicated the presence of two fault systems, trending in the NW-SE direction (Red sea) and NE-SW (Aqaba trend). The RTP map is marked by negative anomaly. A strong NE-SW trending anomaly truncated by the E-W trending is observed in the north-eastern and central parts of study area.

The variations in gravity anomalies were normally caused by variations in the density of subsurface rocks (Reynolds, 1997), and they usually indicated faults or lithological contacts. The Bouguer anomaly map of the study area (Figure 3) was generally in good coverage and it showed gravity values between +50 and -30 mGal. It is characterized by a group of positive and negative anomalies of different intensities and almost NE-SW, NW-SE and E-W orientation. The strongest positive gravity anomalies (50 mGal intensity) lie at the NW and SW corners of



A —— A' Profiles used for interpretations
----- Interpreted fault lines

Figure 4. RTP anomaly map of the study area showing profiles and deduced fault trends.

the study area which associated with the Natash volcanic and the granitic rocks and is separated from the negative gravity anomaly by a very steep gradient. This steep gradient is of NNW trend and could be interpreted to be a normal fault down-throwing to the east. On the other hand the eastern side of the concerned area there is a large high negative anomaly (-30mGal intensity) trending NNE-SSW, associated with the Qena clastics and the limestone. This lithological variation on both sides of the fault as well as the magnitude of fault throw being upthrown to the west is behind the strong difference in the intensity of both positive and negative gravity on both sides of the fault.

a) Trend analysis

Other treatments of Potential Field data include trend analysis to delineate the subsurface fault trends based on the theory of **Grant & West (1965)** and on the **Linsler technique (1967)**, the first horizontal gradient method was applied to all RTP magnetic and the gravity maps. The peaks of the gradient curve were plotted along profiles covering these maps, and

then connected together to show the deduced structure lines.

Close investigations of these maps (Figures 3 and 4) indicate that there are three main structural elements which aligned in direction that bounded both magnetic and gravity anomalies. These elements can be grouped in the following zones:

- 1) The NNW-SSE (Red Sea-Gulf of Suez trend) structural direction as the main structural elements occupying the central and the southern parts of the study area.
- 2) The NNE-SSW (The Gulf of Aqaba-Dead Sea trend) structural direction with less abundance in both maps. This trend located at the northern and southern parts of the area.
- 3) The WNW-ESE (Najd Fault System) structural direction which lying in the northern and southern corners of the study area which is the least prevailing fault system.

b) Werner deconvolution method:

Werner (1953) developed a method for identifying the geometry of magnetization contrasts based on successive determinations of small dikes with infinite strike length and depth extent, perpendicular to the measurement profiles, and which could be considered the source of the magnetic anomaly described by a set of four or more contiguous measurements. The basic expression for the magnetic anomaly of a single dike is:

$$T(x) = \frac{A(x - x_0) + B_z}{(x - x_0)^2 + z^2} \quad (1)$$

where x_0 is the location of the magnetic step, z is the depth to the top, A and B are field functions to be determined, and x is the location at which we want to compute the magnetic anomaly. When several determinations cluster close to a specific location, we infer that the model describes the magnetic interface well. This approach was used

by **Ku and Sharp (1983)**, in a method that has high computational efficiency.

We applied the Werner deconvolution method along set of profiles A-A' of the aeromagnetic map and G-G' of the gravity map. Using clustering method. The outcomes from application clustering method allow us to show the interfaces of the subsurface structures for the aeromagnetic and gravity profiles. The deduced results (see Figure 5a and 5b) illustrated the exact depth of the magnetic and gravity sources where Werner solutions are clustering to each other. Analysis of these profiles showed that the depth to the basement ranges between 1.5 to 0.3km, which is nearly close to the depth of the volcanics deduced by Elawadi and Ismail (2006). The shallowest depths are found at the northern and southern parts of the study area where Natash volcanics and granitic rocks outcrop while the deepest parts occupy the central and western parts of the area where the Nubian sandstone and Qouseir clasts are found.

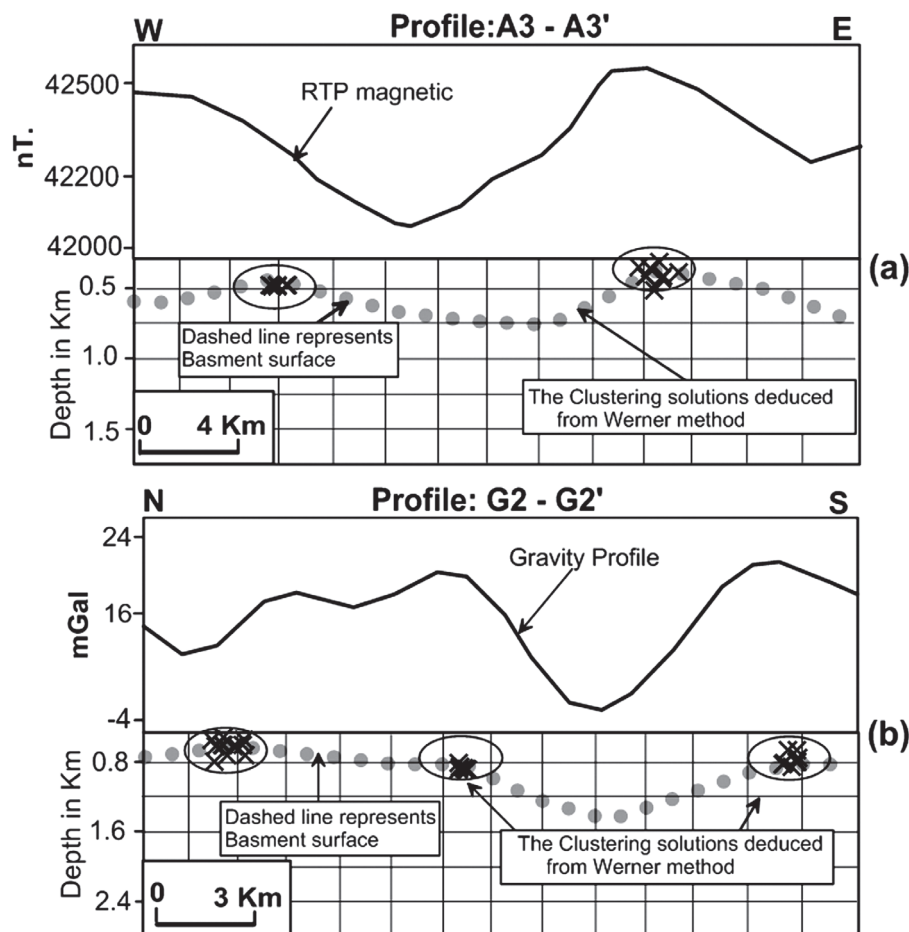


Figure 5. Werner deconvolution showing the depth to the basement rocks and the subsurface structures along Profiles; a) A3-A3' (location shown in Figure 4). b) G2-G2' (location shown in Figure 3).

c) Euler deconvolution method

The Euler deconvolution method delineates geological boundaries of magnetization or density and gives estimates of depth to the basement. Also, this method can be used to determine the subsurface structures (Grauch, *et al.*, 2001). Neil (1990) and Neil *et al.* (1991) applied this technique to magnetic data at Leeds. Few gravity applications have been reported. In this study the application of this technique to both gravity and magnetic data were attempted. The method was originally devised by Thompson (1982) for profile data and later developed for 3D gridded data by Reid *et al.* (1990).

The Euler deconvolution method was applied to the total field intensity along a set of profiles used for aeromagnetic and gravity interpretations (Figures 3 and 4). The windows size used in the process was 11 with applying the suitable dimensions of coordinates. The window slides and the solutions were calculated. The output of this method was representing by the horizontal and Euler solutions. Reid (2003) explained the significance of the deduced structural indices and listed them in Table (1).

Table 1. Structural indices of Euler, after Reid (2003).

Source Type	SI
Sphere or compact body at a distance	3
cylindrical pipe	2
Thin sheet edge (sill, dike, etc.)	1
Fault (small step)	0

The horizontal gradient was used to confirm the deduced subsurface structures. The peaks along these profiles illustrate the location of these structures. It can be noticed, that Euler solutions are clustering along these structures (Figures 6 and 7). Also It can be noticed that the most suitable structural indices (SI) representing the magnetic structures are restricted between 2 and 4 SI indicating an intruded magnetic bodies.

The results from the both magnetic and gravity profiles A2-A2' and G3-G3' (Figures 6 and 7) show that the Natash volcanic extends to a relatively shallow depth (300-100) meanwhile the faults which may be the cause of this volcanic trending NE-SW with depth reaching

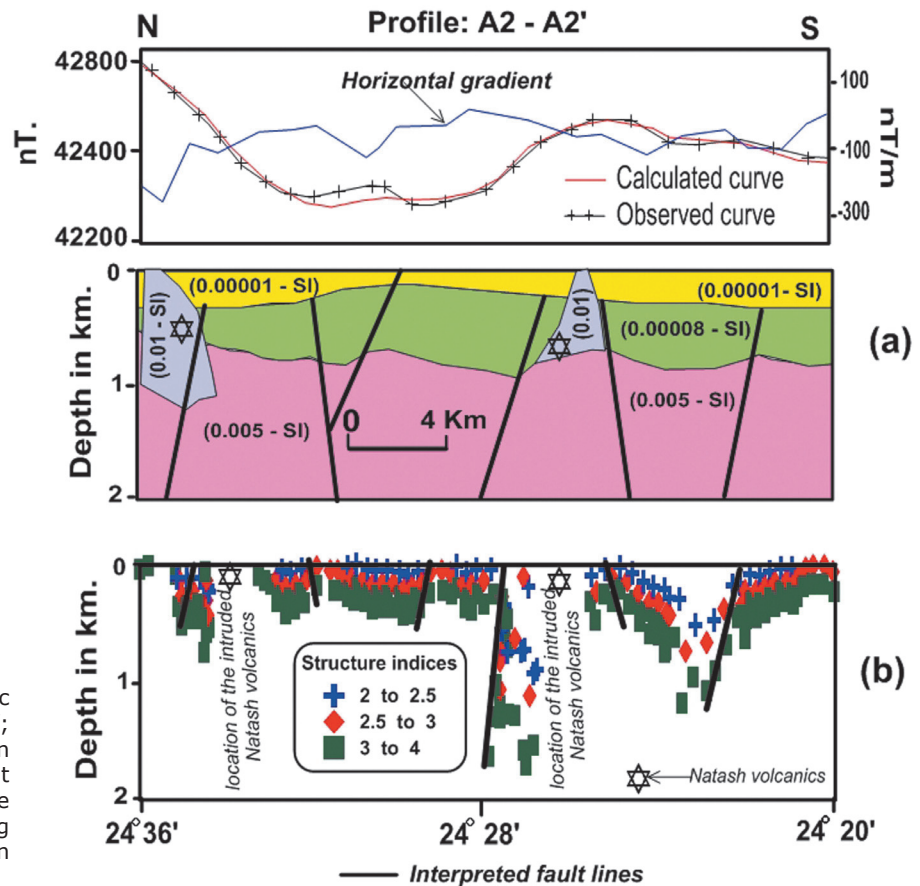


Figure 6. a) 3-D magnetic model for the Profile A2-A2'; b) 2-D Euler deconvolution and horizontal gradient confirming presence of the two fault systems along Profile A2-A2' (location shown in Figure 4).

more than 2km. It is noteworthy that this geophysical subsurface interpretation coincides with the geophysical results by El Gammal *et al* (2013).

d): 3D magnetic modeling

The magnetic field \mathbf{A} at any external point \mathbf{r} due to a volume V of rock which is magnetized with a dipole moment per unit volume \mathbf{M} (**Grant and West, 1965**) is:

$$\mathbf{A}(\mathbf{r}) = \nabla \int_V \mathbf{M} \cdot \nabla [1/(\|\mathbf{r} - \mathbf{r}_0\|) d^3 r_0] \quad (2)$$

Where: \int_V is a volume integration over the body, \mathbf{r} is the distance restricted to the xz plane and \mathbf{r}_0 is the distance from point \mathbf{A} to the centre of the magnetic body.

If the magnetic body is not uniformly magnetized then the extent of the body is between y and $-y$ axis and the observation points will be made along the x -axis across the middle of the body. Therefore, the three components of the magnetic intensity shall henceforth be referred to as the magnetic anomaly given by equation (2) for the magnetic body is:

$$A_x = 2M_x P_x + 2M_z Q, A_y = -2M_y R \text{ and } A_z = 2M_x Q - 2M_z P_z.$$

Where:

$$P_x = a^2 U / a x^2, P_z = -a^2 U / a z^2, R = -a^2 U / a y^2 \text{ and } Q = -a^2 U / a x a z^2$$

and U is the Newtonian potential expressed by:

$$U = 1/2 \int_V M \cdot \nabla [1/(\|\mathbf{r} - \mathbf{r}_0\|) d^3 r_0] \quad (3)$$

Based on **Grant and West**, (1965) and **Talwani** (1960) theories, the 3D modeling technique was applied to the magnetic data using **Encom ModelVision Pro (2004)** software. The technique was applied to the set of aeromagnetic and gravity profiles with different direction covering almost the area (Figures 3 and 4). Inspection of the magnetic profile (Figure 6) revealed that it composed of four bodies representing different lithological and tectonic units. The profile trending N-S showing the highest susceptibility unite (0.01 SI) representing Natash volcanic in the northern and southeastern parts of the profile, reflecting the prevailing fault trends NNW and NNE.

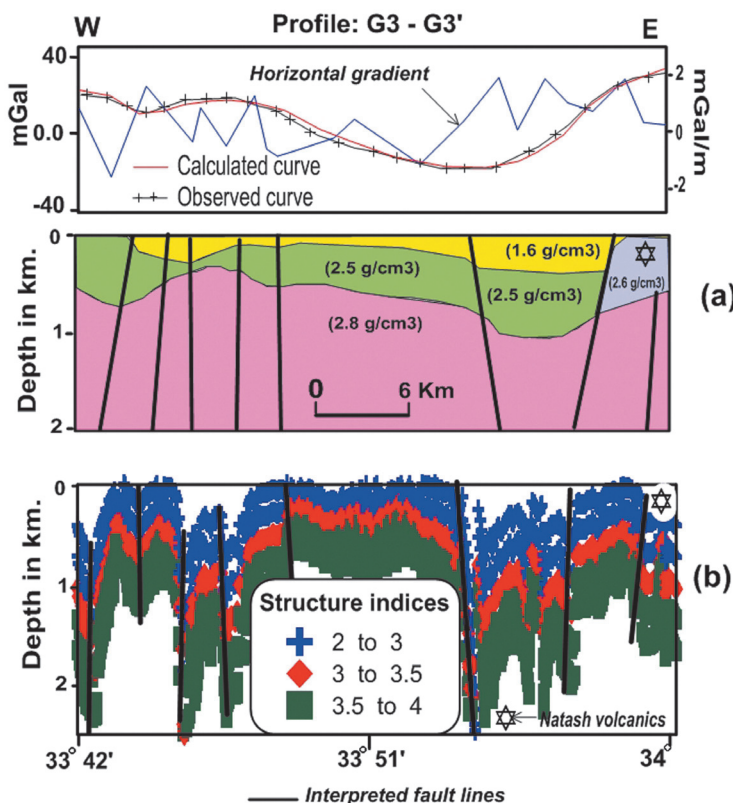


Figure 7. a) 3-D gravity model for the Profile G3-G3'; b) 2-D Euler deconvolution and horizontal gradient confirming presence of the two fault systems along Profile G3-G3' (location shown in Figure 3).

Meanwhile, model for gravity (fig.7) consists of four bodies representing different lithological and tectonic units. This model shows the high density block ($2.6\text{g}/\text{cm}^3$) representing Natash volcanic located at the eastern part of the modeled area. The two fault systems trending NNW and NNE are clearly found with reaching a depth of more than 2km.

The interpreted structural features coincide with the Euler deconvolution of the same trend.

e) Interpreted Structural map with prospected radioactive areas:

Using the radioactive minerals map (Figure 8) established by Elawadi *et al.* (2004) we were able to detect two zones with high concentration of radioactive minerals accumulations. They stated that the radioactive anomalies have been interpreted in younger granites and in adjacent the Nubian sandstones under Wadi Natash exhibits of strong radiometric responses and can be a good target for further mineral explorations. The radiometric data indicate that the granitoid rocks are larger than that present in the geologic map and indicate presence of emanations of radioactive minerals from granites to the surrounding metamorphic rocks due to contact metamorphism. These data indicate that dykes cause a zone of radiometric potential in the surrounding sedimentary rocks (El Gammal, *et al.*, 2013).

The regional tectonic framework of the studied area (Figure 9) was established using the integration of all results of interpretation of the aeromagnetic and gravity analyses, in

addition to the horizontal gradient method in which the peaks of the curves were plotted and connected together to show the possible structural fault lines affecting the study area. Also the 3D modeling to detect the subsurface structures and the depth to the basement rocks (figs 6&7). Visual inspection of the Potential Field data indicated that the most dominant trend in the area is of NNW-SSE related to the Red Sea- Gulf of Suez tectonic trend dissected by the second dominant one trending NNE-SSW related to the Gulf of Aqaba-Dead Sea trend and the WNW-ESE related to the Najd Fault System trend with less contribution in the area under consideration.

The NNW-SSE fault trends are connected with the Red Sea rifting. They occupy the detected zones of high radioactive minerals accumulations (Figure 9). According to Elawadi *et al.* (2004), the Qouseir clastics zone is characterized by radioactive Uranium minerals. Thus we can conclude that the radioactive zones are connected with the Red Sea tectonics and the intruded granitic rocks. The NNW-SSE major faults are controlling the hydrothermal solutions associated with the intrusion of granitic rocks and may be the cause of the formation of radioactive minerals.

Conclusion

The Bouguer, Magnetic and RTP anomalies maps are used to delineate the subsurface structural features prevailed in the study area. They were interpreted using trend analysis, 2D Euler deconvolution, Werner deconvolution and 3D modeling techniques. The results show that

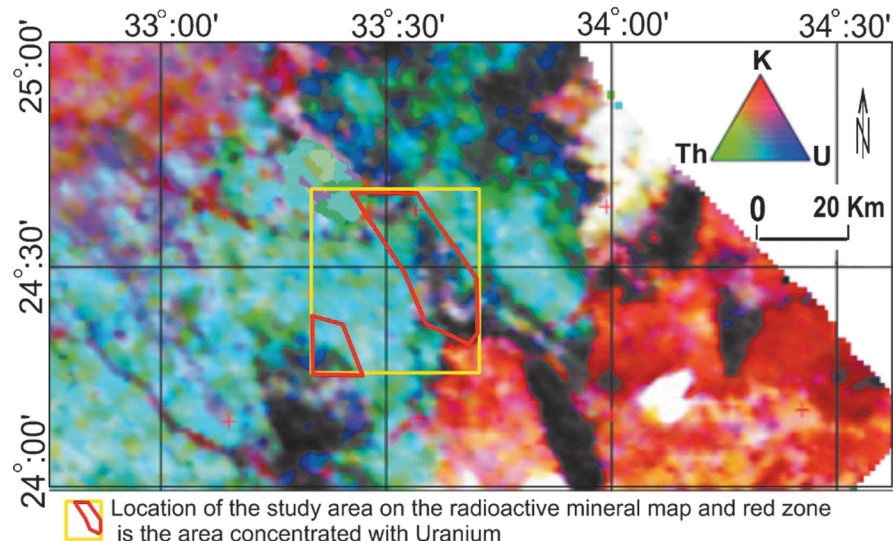


Figure 8. Radioelement composite image (after Elawadi *et al.* 2004) showing zones with radioactive minerals accumulations.

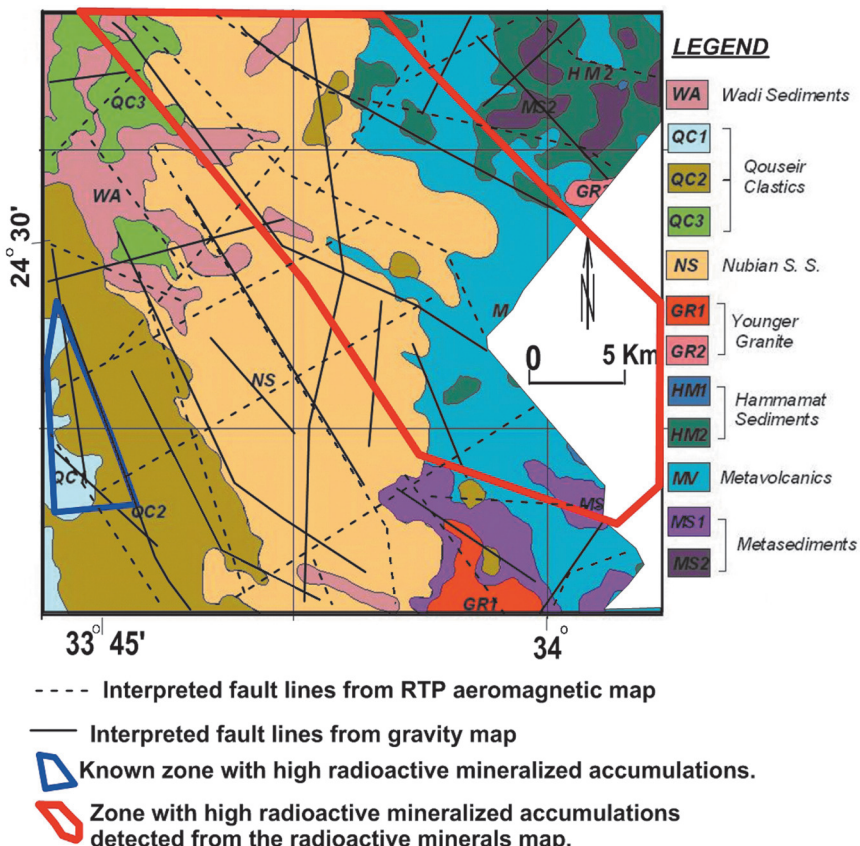


Figure 9. The interpreted basement tectonic map with promising location of radioactive elements.

the area is structurally controlled by major faults trending in the NNW-SSE direction related to the Red Sea tectonics. They are intersected by the less predominant fault structures which have NNE-SSW and WNW-ESE directions.

The study area was affected by mass granitic rock intrusions. The depths to the intruded rocks reach from 300m to 1500m. The Natash volcanic is intruded to granitic rocks and overlying Qousuir clastics and Nubian sandstone. The integrated results from gravity, magnetic and radiometry indicate the relationship between the NNW-SSE fault trends and intruded granitic rocks as well as the radioactive mineral accumulations exists. From the results deduced from all the interpretations and analyses techniques applied to both magnetic and gravity data, it can be concluded that the Qousuir clastics and the Nubian sandstone rocks were affected by the intrusion of the Natash volcanic which is post rifting the Red Sea and it would form radioactive mineral accumulation as a result of hydrothermal solution. The NNW-SSE fault trends act as path channels for these solutions rich with radioactive minerals.

References

Aero-Service, 1984, Final operational report of airborne magnetic/radiation survey in the Eastern Desert, Egypt. For the Egyptian General Petroleum Corporation (EGPC) and the Egyptian Geological Survey and Mining Authority (EGSMA). Aero-Service Division, Houston, Texas, USA, Six Volumes.

Conoco and Egyptian General Petroleum Corporation, 1987. Geological map of Egypt, Scale 1:500,000, Cairo.

Conoco Inc., 1989, Stratigraphic lexicon and explanatory notes to the geological map of Egypt 1:500,000. Conoco Inc., Cairo, Egypt, P. 262.

Crawford W.A., Coulter D.H., Hubbard J.H.B., 1982, Wadi Natash olivine alkali basalt volcanic series a harbinger of Red Sea rifting, *Geol. Soc. Am.*, 14, 469.

Crawford W.A., Coulter D.H., Hubbard J.H.B., 1984, The aerial distribution, stratigraphy and major element chemistry of Wadi Natash volcanic series, Eastern Desert, *Egypt. J. Afr. Earth Sci.*, 2, pp. 119-128.

El Gammal, El Sayed A., Salem S.M., Greiling Reinhard O., 2013, Geology, Morphotectonics And Geophysical Interpretation Of Wadi Garara Graben, East Aswan Egypt, Using Landsat Images. *Australian Journal of Basic and Applied Sciences*, 7, 1, pp. 263-277.

Elawadi Eslam A., Ismail Atef A., 2006, Aeromagnetic imaging of Wadi Natash volcanics, South Eastern Desert, Egypt. submitted to the 8th SEGJ conference, Kyoto, Japan.

Elawadi E., Ammar A., Elsirafy A., 2004, Mapping surface geology using airborne gamma-ray spectrometric survey data- A case study, Proceedings of the 7th SEGJ International Symposium, Japan, November 24-26, 2004.

Encom ModelVision Pro, 2004, software for PC developed and supported by Encom Technology Pty Ltd. Version 6.00 September 2004: Head Office Level 2, 118 Alfred St, Milsons Point, New South Wales, Australia 2061.

Grant F.S., West G.F., 1965, Interpretation theory in applied geophysics, MacGraw- Hill, pp. 584-588.

Grauch V.J.S., Hudson M.R., Minor S.A., 2001, Aeromagnetic expression offaults that offset basin fill, Albuquerque Basin, New Mexico: *Geophysics*, 66, 707-720.

Hashad A.H., Hassan M.A., Aboul Gadayel A.A. 1982, Geologicol and petrological study of wad. Natash late Cretaceous volcanic, Egypt. *J. Geol.*, 26, pp. 19 – 37.

Ibrahim M.E., 2010, Laterites Bearing-REEs, Wadi Natash, Southeastern Desert, Egypt. *Journal of Rare Earth*, 28, 3, pp. 471-476.

Ku C.C., Sharp J.A., 1983, Werner deconvolution for automated magnetic interpretation and its refinement using Marquardt's inverse modeling, *Geophysics*, 48, pp. 754 - 774.

Linsler H., 1967, Investigation of tectonics by gravity detailing. *Geophysical Prospecting*, 15.

Neil C., 1990, A computer program to interpret automatically potential field data using Euler's equation of homogeneity: Unpublished M.Sc. thesis, University of Leeds, 72p.

Neil C., Whaler K.A., Reid A.B., 1991, Extensions to Euler's method for three-dimensional potential field interpretation: (Abstract) Presented at EAEG, Florence.

Noweir A.M., Lebda E.M., Noweir M.A., Nassim A.S., Elkholiey E.M., 2003, Tectonic evolution geochemistry and petrogenesis of the alkaline volcanic rocks of Wadi Natash, Egypt. *Jour. Geol.*, 47, pp. 541-568.

Reid A.B., Allsop J.M., Granser H., Millett A.J., Somerton I.W., 1990, Magnetic interpretation in three dimensions using Euler deconvolution, *Geophysics*, 55, 1, pp. 80-91.

Reid A.B., 2003, Euler magnetic structural index of a thin-bed fault. *Geophysics*, 68, 1255-1256.

Ressetar R.D., Nairn A.E.M., Monrad J.R., 1981, Two phases of Cretaceous- Tertiary magmatism in the Eastern Desert of Egypt: paleomagnetic, chemical an K-Ar evidence. *Tectonophysics*, 73, pp. 169-193.

Reynolds John M., 1997, An Introduction to Applied and Environmental Geophysics. John Wileyand Sons, Ltd. New York.

Richard J. Blakely, 1995, Potential Theory in Gravity and Magnetic Applications, Cambridge University Press, New York, P. 441.

Sandwell D.T., Smith W.H.F., 1997, Marine gravity anomaly from Geosat and ERS-1satellite altimetry. *J. Geophys. Res.* 102, 10039–10050 available at http://topex.ucsd.edu/cgi-bin/get_data.cgi.

SURFER, 2002, Surfer® Version 8.00, Feb 11, 2002 (Golden Software Inc., Golden, CO, U.S.A.).

Talwani M., 1960, Rapid computation of gravitational and Ewing, M. attraction of three-dimensional bodies of arbitrary shape. *Geophys.*, 25, pp. 203-225.

Thompson D.T., 1982, EULDPH – A new technique for making computer-assisted depth estimates from magnetic data. *Geophysics*, 47, 31 – 37.

Werner S., 1953, Interpretation of magnetic anomalies at sheet-like bodies. *Sveriges Geologiska Undersöknings 43.C* – 2009 University of Lisbon, *Geophysical Prospecting*, 57, 447–459.